Starshade Technology Development Activity Milestone 8A

Verify Petal Position On-Orbit Stability

David Webb, S. Case Bradford, John Steeves, Doug Lisman,

Jet Propulsion Laboratory, California Institute of Technology, Pasadena CA

David Opland, Gregg Freebury,

Tendeg, Louisville CO

Jeremy Senne, Charles Tan, Aaron Armour,

Applied Composites, San Diego CA

Jamie Abbott,

JLA, San Diego CA

Siu-Chun Lee and Larry Chan

Applied Sciences Lab, Inc., Baldwin Park CA

CONTENTS:

Executive Summary

We demonstrate compliance with S5 Milestone 8a with large margin, which concerns the on-orbit thermal stability of the truss-bay longeron and node assemblies of the Inner Disk Subsystem (IDS), over the full range of observational sun angles. Maximum expected thermally induced disk radius error versus sun angle was predicted via a system model that included validated component-level analysis models of the longerons and nodes, and demonstrated large margin relative to all error budget sub-allocations. The analysis models were validated at the component prototype level via dimension versus temperature measurements of full-scale, medium fidelity, prototype test articles of the longeron and node assemblies that included the dimension critical features. The ideal disk radius for the thermal environment was determined, which was the basis of comparison for the actual disk radius performance, which included a maximum expected performance error that resulted from an industry partner's material properties and manufacturing tolerance error study, and also included a temperature prediction error.

JPL, Tendeg, and Applied Composites performed the design, analysis and fabrication of the prototypes and test articles that were designed to fit within Northrop Grumman's Interferometric Metrology Facility (IMF) for dimension versus temperature test. This test data was used to compare to the model predictions.

1 Introduction

This report details the S5 efforts to verify starshade Inner Disk Subsystem (IDS) on-orbit thermal stability performance (KPP 8) and is intended to close out the S5 technology milestone 8A, which reads:

> *Truss-bay longeron and node sub-assemblies demonstrate on-orbit thermal stability within ± 200 microns by analysis using a validated model of critical dimension vs. temperature.*

This specification applies as the difference between the *actual* petal position and the *ideal* petal position, in the thermal environment. The ideal petal position (disk radius) is that which minimizes the difference between the thermal strain of the petal and the disk. More specifically, it is the petal width dimension that is critical (as opposed to the length), because it is the dominant parameter for instrument contrast performance. A more thorough explanation of this can be found in Appendix A.

Truss-bay longerons and nodes comprise the perimeter truss circumference, and thus determine the disk radius. The random variations of each truss bay in the thermal environment are the root cause of the random and tangential errors that the sub-allocations cover. The radial bias is the average radius that results from the aggregate of the random variations of the individual bays.

To enable parallel development of the truss and petal, the ideal disk radius, as a function of sun angle, is established at program start. The petal and disk errors are then sub-allocated relative to this ideal. This specification applies over a 40° to 83° range of star-sun angle thermal environments (henceforth called sun angles), that envelop the HabEx and WFIRST-Starshade Rendezvous Mission (SRM) cases. Table 1-1 shows truss-bay error budget sub-allocations to radial-bias, radial-random and tangential-random error components. The table includes two types of contrast contributions. The radial-bias term is the contrast evaluated at the maximum allowable radial shape error of ± 50 µm, and applies across the entire observational sun angle range. Unless otherwise specified, the contrast shown is the mean value for a normal distribution with the specified 3-sigma standard deviation of the engineering parameter. When a 'do not exceed' value is listed, the contrast shown has been evaluated at the do-not-exceed value of the parameter. Petal shape stability is the subject of milestone 6a.

Table 1-1 Milestone 8a sub-allocations. Radial is with respect to the center of the starshade 2-d planar shape, and tangential is with respect to the circumference of the center opaque disk.

Sub-allocation term:	**Shape Error (µm)**	**Instrument Contrast**
Radial-bias (uniform)	50 (do not exceed)	8.50E-13
Radial-random (bay to bay)	96 (3σ)	6.13E-14
Tangential-random (bay to bay)	96 (3σ)	9.29E-14
Totals	**145 (RSS Total)**	**1.00E-12 (Linear Sum)**

To establish the ideal disk radius for the thermal environment (sun angle range), the thermal strain in the petal width dimension was modelled at discrete sun angles, and the ideal disk radius for each sun angle was determined from this. Then, the truss-bay longeron and node assemblies are carefully designed to minimize the difference between the actual disk radius and the ideal, across the observational sun angle range. It should be noted that milestone 6a also has a sub-allocation for the error between the actual petal prototype and the modelled value. Future activities will iterate on the hardware designs to minimize the error, but this activity is schedule limited to a single design cycle.

The milestone demonstration approach is to develop a validated model to predict the thermal stability performance of the perimeter truss longerons and nodes as a function of the observational sun angle thermal environment. We then add to this validated model performance prediction, a max expected error in performance due to quantifiable material property variations and manufacturing tolerances, as well as the uncertainty in the on-orbit temperature prediction. This establishes a maximum expected total error in performance. We then conservatively compare this max expected error to the radial bias sub-allocation of ± 50 μm, which is the equivalent of assuming *all* longerons and nodes are at the extreme of the max expected error. In constraining ourselves to this tighter requirement, the random error sub-allocations are also satisfied.

The model validation approach is to precisely measure the critical dimension versus temperature of test articles for the truss-bay longeron and node assemblies. Available test facilities limit test article dimensions and geometry. Medium fidelity longeron prototypes include all dimension critical features and are produced at full-scale, but then cut into 3 test articles to fit in the selected facility. A medium fidelity node assembly prototype is produced; however, because it is not flat, the critical dimension cannot be measured in the available facilities. Instead, we cut out and test the center-brace portion of the assembly, which dominates the length of the critical dimension of the node assembly. We also build and test multiple pin-bushing joint assemblies as-bonded to the node plate. Note that milestone 8b will demonstrate this same performance enumerated in Table 1-1 for an integrated truss-bay, but will be tested in a custom metrology setup capable of testing an entire truss bay.

The remainder of this document is organized as follows. Section 2 presents the flight mechanical architecture/design, thermal environment/analysis and an error bounding study from which max expected performance error uncertainty is derived. Section 3 describes the model validation approach, test facility, test articles and component level test results. Section 4 describes flight design modeling. Section 5 presents the predicted on-orbit system performance and compares it to the milestone, along with conclusions and plans for future work.

2 Flight Design

2.1 Flight Mechanical Architecture

The Starshade is a deployable structure that has three subsystems, the inner disk, the petal, and the petal launch restrain and unfurl subsystem (PLUS), see Figure 2-1. The petals and truss are designed to be deployed independently, in a two-phase deployment. First, the PLUS quasi-statically releases the petals from their furled (launch) condition, then the truss launch locks are released, and the truss deploys the petals passively to their design diameter. The PLUS is jettisoned after unfurling the petals, and does not contribute to on-orbit stability.

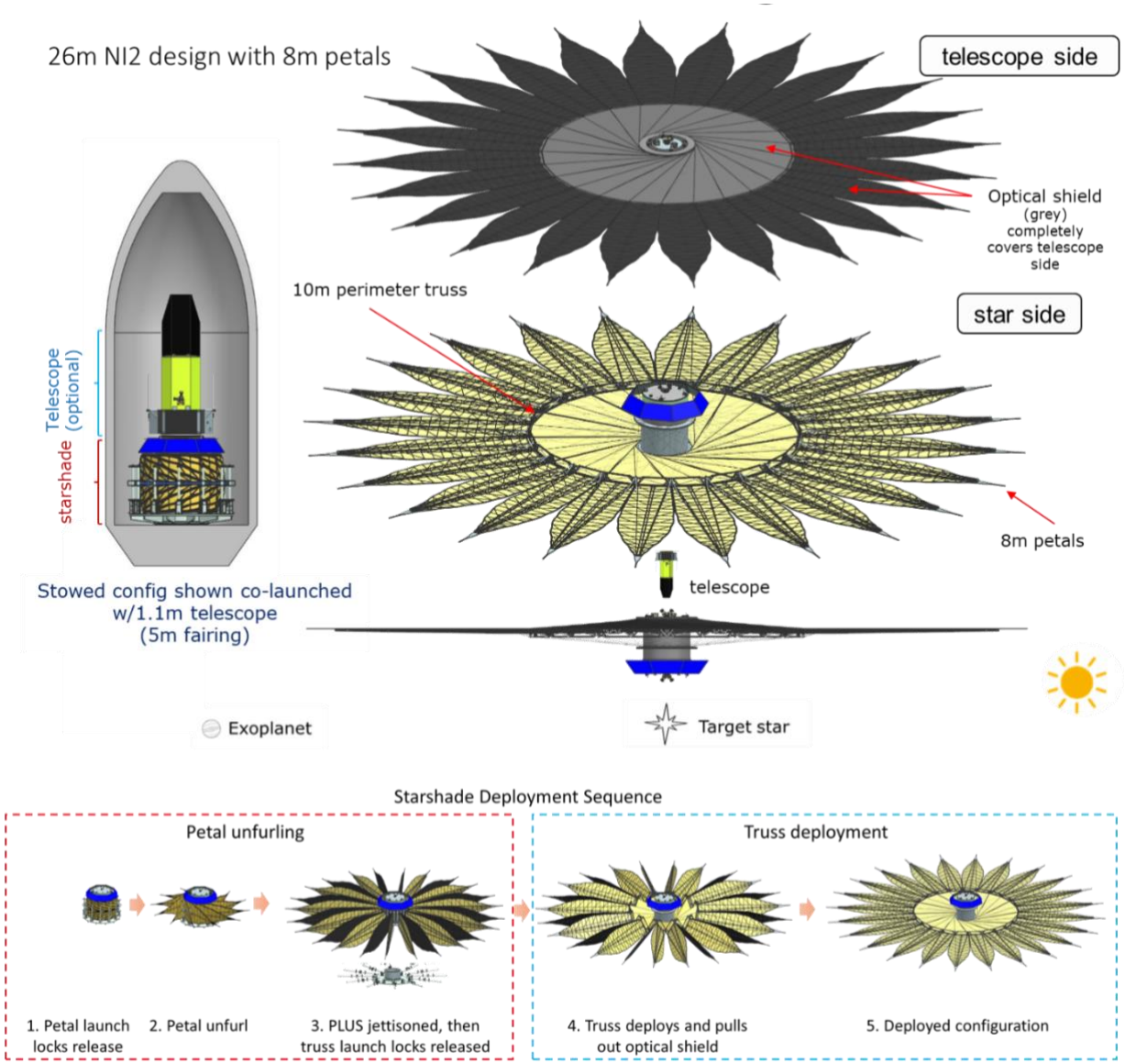

Figure 2-1. Starshade mechanical system including deployed and stowed configuration with relative position of starshade, telescope and star (top). Deployment sequence for the starshade, beginning with petal unfurling, and completing with deployment of the perimeter truss (bottom).

Part of the on-orbit stability design is to minimize load coupling between the petal and disk, which reinforces the error budget breakdown of petal position and petal shape as independent

parameters. The actual interfaces are of course non-ideal, but their detailed designs are included in the hardware, and their coupling is present in the analysis models. The focus of this milestone is the inner disk on-orbit thermal stability, specifically the perimeter truss. For a more detailed description of all starshade subsystems and the deployment sequence, see the Probe Study [2] and HabEx reports [3]. The on-orbit thermal stability of the petal is discussed in milestone 6a report.

2.1.1 Perimeter Truss

The perimeter truss is designed to deploy and latch independently of the petal, and has a clean, bolted interface for the petal hinges. This allows the perimeter truss to be designed and analyzed independently of the petal. The coupling effects that do occur are present in the system level analysis model, although to first order, the petal does not influence inner disk on-orbit stability. The 10-m perimeter truss design presented herein, Figure 2-2, is specifically designed to scale up to the 20-m truss that the HabEx design utilizes [4]; there are no architectural differences between the two truss sizes. Analysis has been performed and presented in the HabEx report that verifies these assumptions.

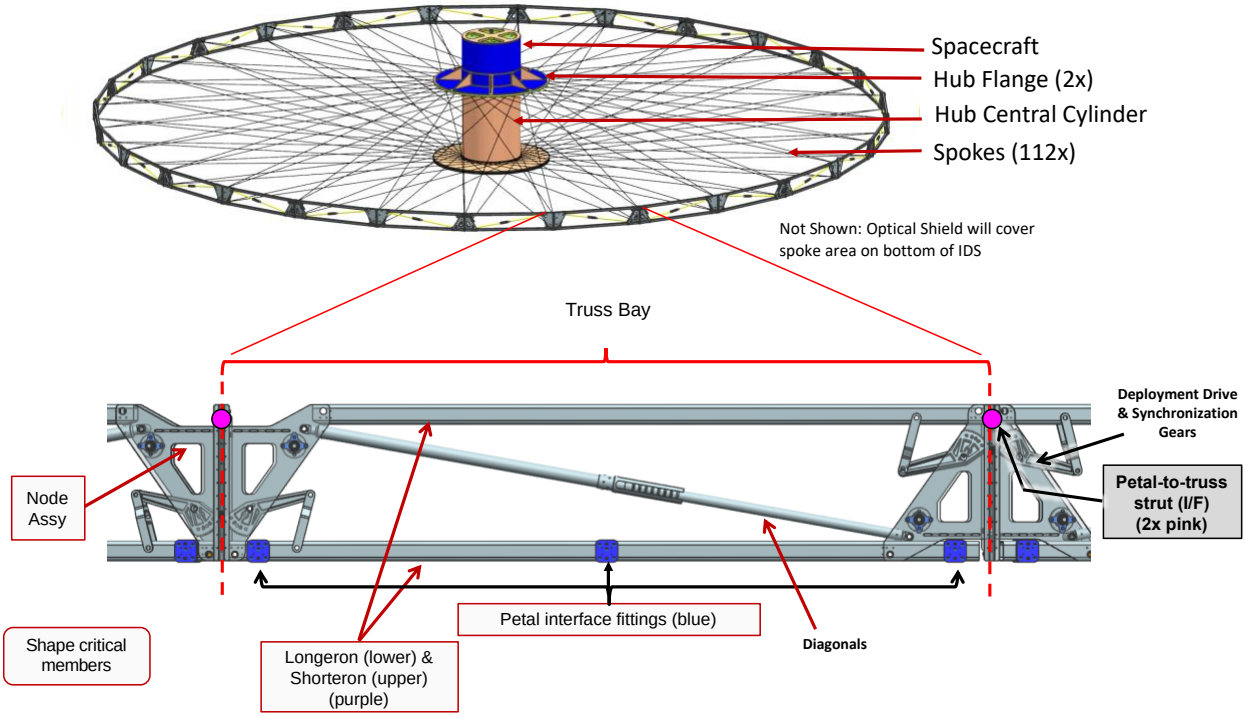

Figure 2-2 Inner disk perimeter truss, spokes and hub (shield suppressed for clarity) detailing the 'truss-bay' and its components. Most importantly for this effort, the longeron and node assemblies are the shape critical components. Note this image represents an earlier prototype of the truss whose high-level details are representative. The as-built and tested prototypes more closely reflect the flight dimensions and geometry with respect to the shape-critical components.

The perimeter truss is a tensegrity structure put into compression via a relatively low 16 lbf. tension in each spoke. The overall shape of the truss and its petal interface points is driven by the circumference of the truss ring. The shape-critical components of the perimeter truss are the longerons and nodes, highlighted in Figure 2-2. It should be pointed out for clarification, that the 'shorteron' and 'longeron' are nearly identical members on opposite sides of the ring. The only difference is that the longeron interfaces to the petal. The shorterons can be made to be exactly identical to the longerons, if that is so desired for thermal stability. For this reason, the longeron will be the focus of this milestone. The deployment mechanisms are out of the load path as-

deployed, and do not contribute to thermal stability. The longerons and nodes are connected via metallic pins through aligning bushing bore holes, and are free to rotate about their axis. The result is that the perimeter truss's thermal deformation response is dominated by the response of the longerons and nodes. Descriptions of the longerons and nodes are in the model validation section of this paper, section 3.3.

2.2 Thermal Environment

The thermal environment on-orbit is a function of the sun orientation with respect to the starshade, defined herein as the angle of the sun with respect to the starshade normal, see Figure 2-3. Observation angles are enveloped by the HabEx mission parameters of sun angle 40° to sun angle 83°. The starshade spins at a rate of 1/3 RPM about its principal axis, which is co-axial with the long axis of the center hub. Sun angles less than 40° will only be experienced during retargeting of the starshade and therefore do not affect thermal stability during observation, and angles greater than 83° are also not expected during observation. It is required that the starshade meet on-orbit shape stability for the given starshade temperature profile resultant from that range of sun angles.

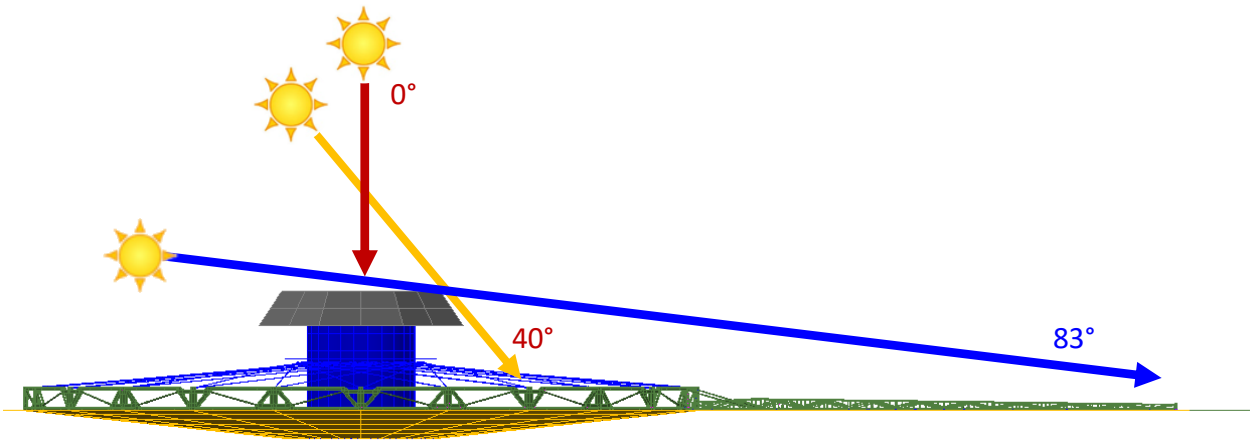

Figure 2-3. Sun angle is defined with respect to starshade normal, which equals a sun angle of 0°. Observation angles are enveloped by the HabEx mission parameters of sun angle 40° to sun angle 83°.

2.2.1 Thermal Analysis Model & Thermal Design

The flight design was modelled in the Thermal Desktop analysis software package; the model can be seen in Figure 2-4. The inner disk, with its perimeter truss, spokes and hub, is well detailed, with all components relevant to thermal performance present. Also attached are two detailed petals, along with 22 'flat', low-detail petal shields that provide the surrounding thermal environment for the detailed petals and truss; this was done to greatly reduce model run time. The effect of detailed vs 'flat' petals for the thermal environment was studied and shown to be a valid assumption. The temperatures of the two detailed petals are evaluated in a transient analysis, and the petals' temperatures are exported to each of the 12 positions around the starshade to obtain the temperature profile of all 24 petals. These temperatures are then mapped to the structural model.

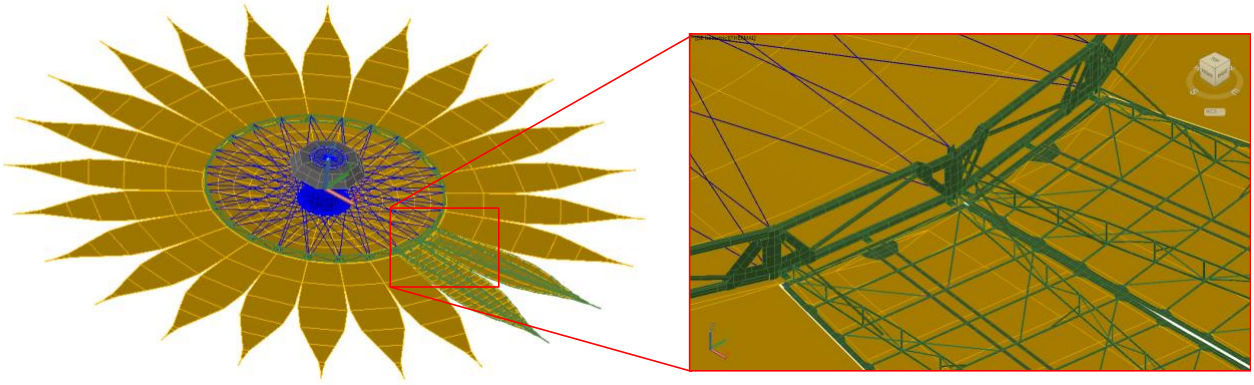

Figure 2-4 Starshade thermal analysis model includes a detailed inner disk including perimeter truss, and two detailed petals that are surrounded by simplified petals that provide an accurate thermal environment.

The thermal design approach of the starshade is centered around cold-biasing the structure, and minimizing the temperature range, resulting in smaller thermal strain variation of the shape critical components. To achieve this, each component in the structure is wrapped, or covered, in a single layer of Silicon-doped Kapton insulation, which is aluminized on the anti-sun side, giving it a low solar radiation absorptivity to emissivity ratio.

2.2.2 Thermal Analysis Results

The starshade spins at a rate of 1/3 RPM, which results in a max variation in the longeron temperature of less than 2 °C through the spin. Sun angles of 40° and 83° represent the hottest and coldest thermal environments over the observation angles for which the starshade must meet thermal stability requirements. Figure 2-5 shows that for sun angle 40°, the longeron and node assemblies have average temperatures of 59 °C and 57 °C, respectively. For sun angle 83°, they have an average temperature of -12 °C and 9 °C, respectively.

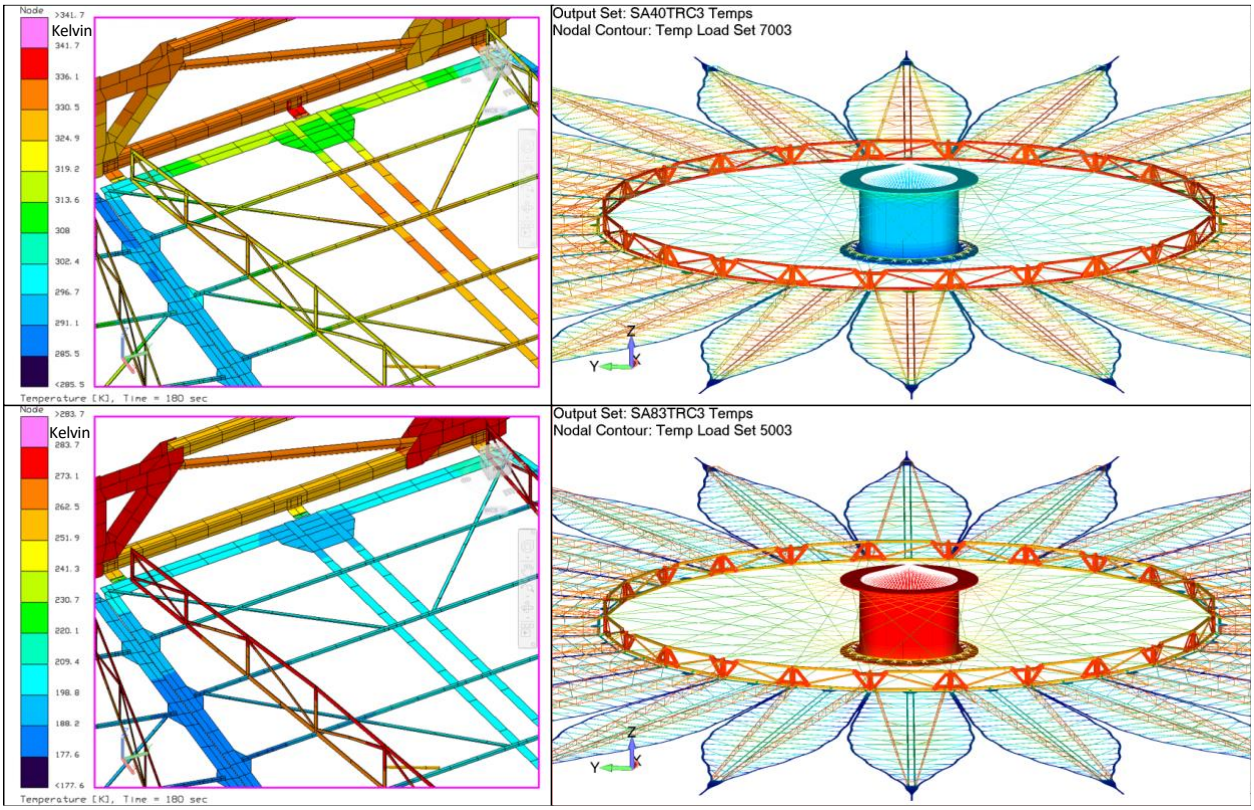

Figure 2-5. Thermal plots for sun angles 40° (top) and 83° (bottom), the extremes of the observation orientations. Note that view orientation is NOT the sun angle. Image of the base of the petal and truss-bay on the left, including longeron and node assemblies with scale bar in Kelvin, and to the right, the entire starshade structure. The longeron and node assemblies have an average temperature of 59 °C and 57 °C for sun angle 40°, and for sun angle 83°, they have an average temperature of -12°C and 9°C, respectively. Note that other starshade details including blanketing are suppressed for clarity.

2.3 Actual Disk Radius Design vs Ideal Disk Radius

Per discussion in section 1, the actual disk radius is designed to best match the ideal disk radius for the thermal environment. To establish the ideal disk radius for the thermal environment (sun angle range), the thermal strain in the petal width dimension was modelled at discrete sun angles, and the ideal disk radius for each sun angle was determined. Then, the truss-bay longeron and node assemblies are carefully designed to minimize the difference between the actual disk radius and the ideal across the observational sun angle range.

To model the thermal strain (the product of delta temperature and coefficient of thermal expansion, or CTE) of the petal width dimension, the industry standard modelling tools of CompositePro and Classical Laminate Theory (CLT) were utilized, with measured and published values for material properties as the inputs. This same material database and software set were used to optimize the design of the longerons and nodes to best match the actual disk radius to the ideal disk radius.

The optimization parameters included: varying the fiber volume fraction (fiber to resin ratio), laminate ply orientations (individual ply stack-up orientations), and geometry of the metallic fittings. Each of these parameters have a significant and deterministic effect on the overall assembly thermal strain as a function of temperature. Figure 2-6 shows the petal design that was modelled for determination of the ideal disk radius.

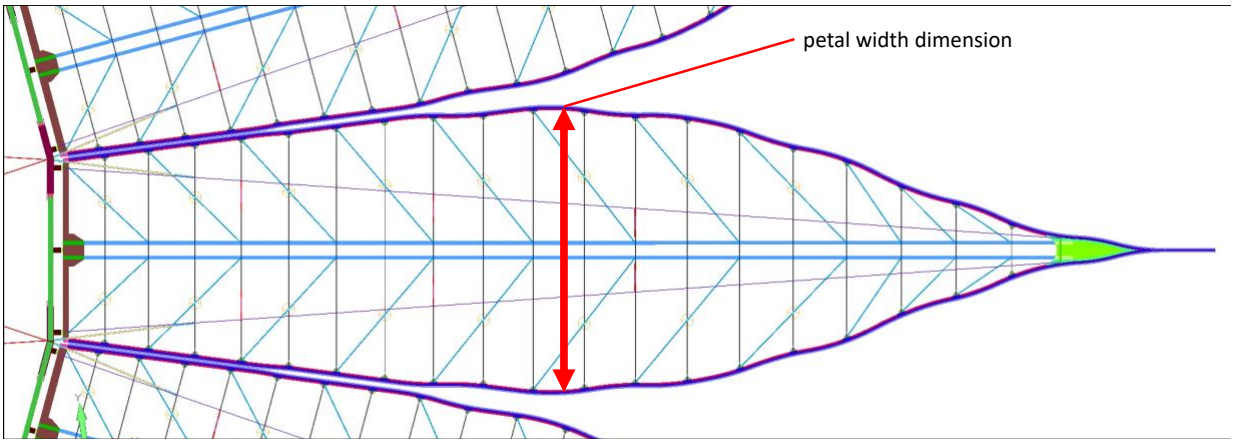

Figure 2-6. Structural analysis model of the petal design that was used to determine the thermal strain performance of the width dimension of the petal as a function of sun angle/temperature for the purpose of determining the ideal disk diameter.

The actual disk radius that results from the longeron and node designs is plotted in Figure 2-7, along with the ideal disk radius. Disk radius thermal distortion is plotted in µm as a function of sun angle in degrees. The milestone requires the difference between the actual and ideal disk radii (the error), be less than ± 50 µm. Thermal distortion is relative to the as-built 20 °C reference temperature. The truss longeron and node are designed to minimize the error between the actual and ideal disk radii.

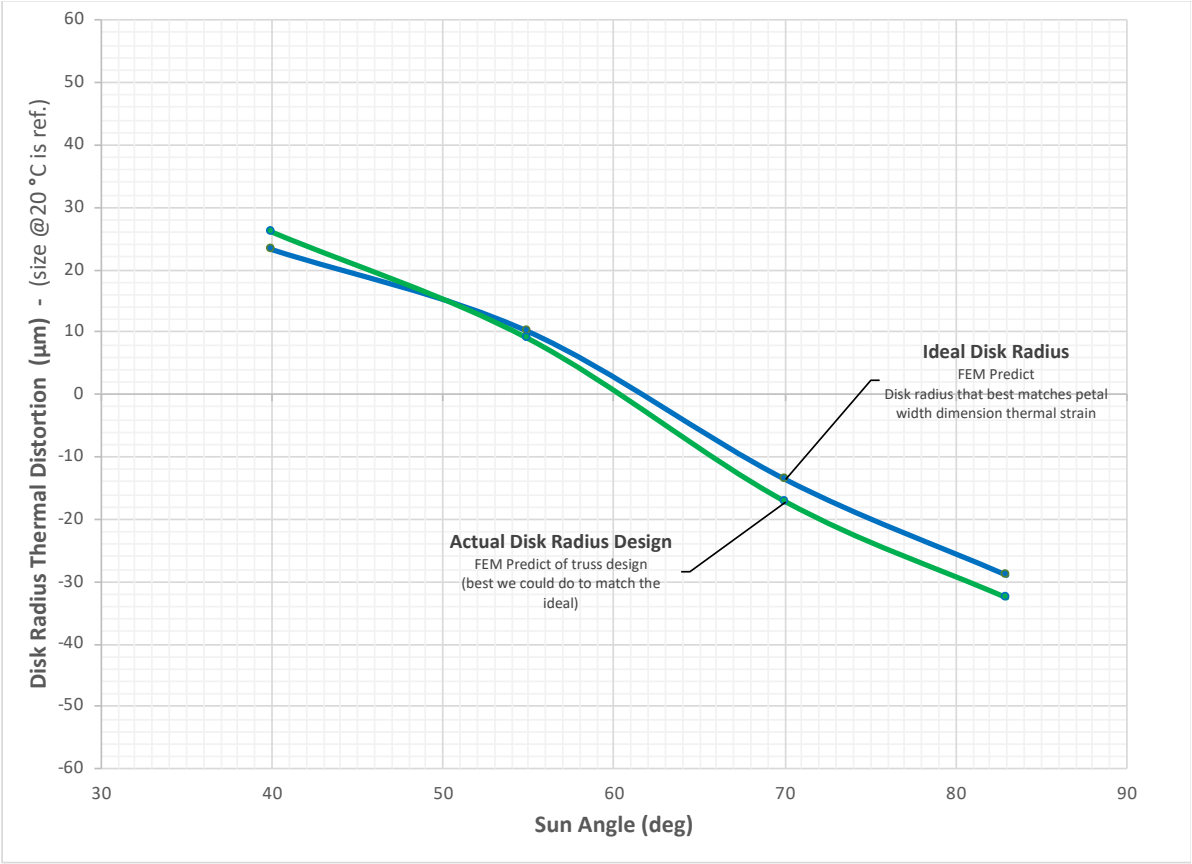

Figure 2-7. Actual disk radius that results from the longeron and node designs along with the ideal disk radius. Disk radius thermal distortion is plotted in µm as a function of sun angle in degrees. Thermal distortion is relative to the as-built 20 °C reference temperature.

Ideally, the actual disk radius would exactly match that of the ideal disk radius. In practice, this is not possible because the constituent materials that comprise the longeron and node are necessarily different than that of the petal, and also because the temperature of the two assemblies are different as a function of sun angle. The goal therefore, is to minimize the difference in thermal strain between the two curves (y-axis of Figure 2-7), across the observational sun angles. The maximum difference between the actual and ideal occurs at the extremal sun angles, where delta thermal strain is at a maximum.

2.4 Max Expected Performance Error

To bound the maximum expected performance error of the actual disk radius with respect to the ideal, we performed a study to establish an upper and lower bound with respect to the actual disk radius design nominal. The maximum error bounds are later used as the criterion for model validation for the prototypes and test articles.

The study varied the analysis inputs and manufacturing parameters that define the thermal stability of the hardware. The analysis is limited by the assumptions, which includes utilizing the average of as-measured material properties from a set of coupons. In fact, the actual material property behavior of the test article is somewhere in the range of the as-measured values; this actual variation in behavior has significant impact on the as-built test hardware. Manufacturing tolerances are equally as important, and in fact represent the majority of the variation in as-manufactured performance.

A study was conducted by an industry partner to understand the various material property and manufacturing parameters that would significantly influence our as-built hardware. Figure 2-8 is the result of that study, and represents their best understanding of the significant parameters, as well as a conservative bounding on the degree to which those values can vary. The result is the differential thermal strain from the nominal design, evaluated at 70 °C, represented along y-axis in parts per million (ppm), with the nominal design being at $y = 0$. For reference, the overall thermal strain of the design is 13 ppm at 70 °C. The largest effects on thermal strain are from ply angle deviations from nominal, fiber volume fraction, lamina modulus, and Poisson's ratio of the lamina.

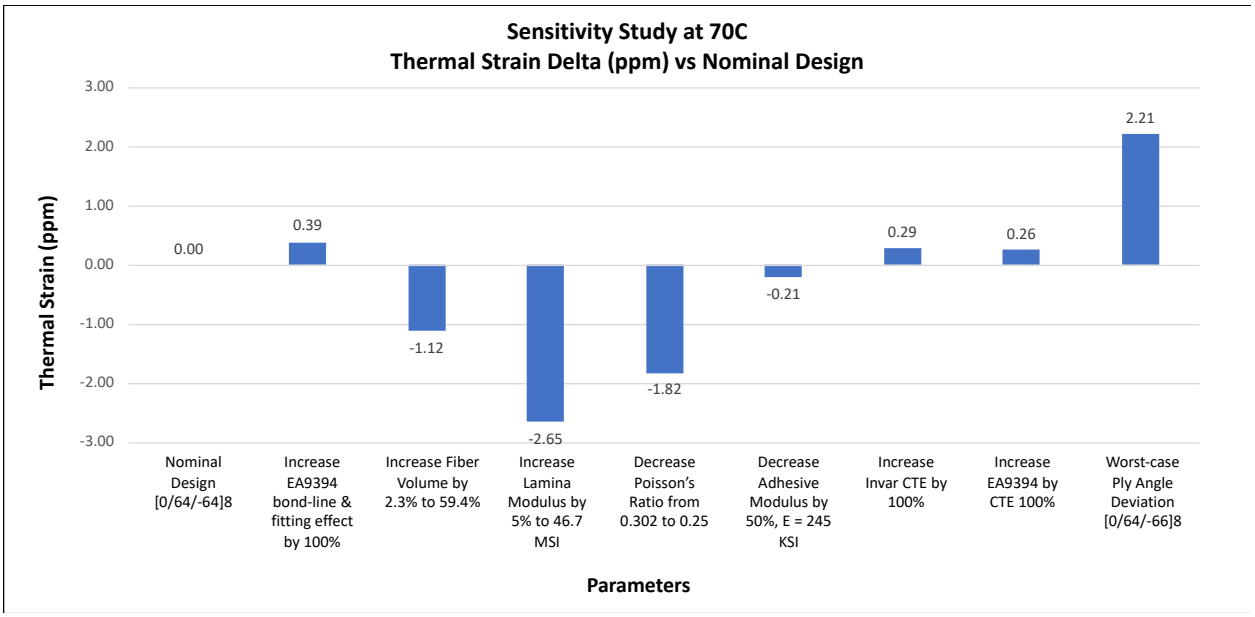

Figure 2-8. Results of study performed by industry partner to bound the max expected error of the as-manufactured hardware from the nominal (measured in thermal strain), due to variation in the material properties and manufacturing tolerances. Each parameter was conservatively varied to understand its impact on performance.

The study parameters here are understood to be independent and uncorrelated in cause, and therefore the results for each parameter can be combined together in quadrature to establish a max expected error of 4.1 ppm from the design. While these uncertainties are meant to bound industry capability and standard material variations, a model uncertainty factor (MUF) of 1.25 has also been applied to capture the general uncertainty associated with working in the margins of industry capability, as well as any unknown unknowns. With the MUF of 1.25, the max expected error is 5.1 ppm from nominal design, and is the value used to bound the longeron and node test article performance individually for model validation.

For the actual disk radius design performance, it is important to also include the uncertainty in temperature of the longeron and node, which could result in those components being hotter or colder than expected. Based on historical data and following the JPL standard approach, we include a temperature prediction uncertainty of ± 10°C. We assume the disk hardware is 10 °C hotter than for the driving case of SA40, and 10 °C colder for SA83. This represents an additional thermal strain delta of 3 ppm at SA40, which we conservatively apply to SA83 as well (10 °C colder at SA83 is only 1 ppm additional strain). The temperature uncertainty of 3 ppm proves to be of similar influence compared to the individual sources of manufacturing error already discussed. The temperature uncertainty is assumed to be uncorrelated to the manufacturing errors, and is combined in quadrature with those to produce a total disk max expected uncertainty of 5.9 ppm. This value defines the max expected error of the actual disk radius, and is applied as a plus/minus tolerance to the actual disk radius performance curve to create the max and min expected error in disk radius performance seen in the milestone analysis in section 5.

3 Longeron & Node Model Validation

3.1 Model Validation Approach

The model validation approach is to precisely measure the critical dimension versus temperature of the key truss-bay test articles, and then verify that the measurement-based predictions of the prototypes are within the maximum expected values. To achieve this, a test facility is selected that is consistent with the desired measurement accuracy, and this facility then imposes constraints on test article dimensions and shape, as detailed in the following sections. An important aspect of this activity was the gradual refinement of all material models as more accurate and relevant test data became available.

3.2 Test Facility

The test facility selected to characterize thermo-elastic deformations is Northrop Grumman's Interferometric Metrology Facility (IMF) in San Diego, California, illustrated in Figure 3-1. The IMF has an accuracy of better than one micron, and accommodates test articles up to 70-cm in length, and several centimeters in cross-section. It can achieve 20K to 450K test-article temperatures for lengths up to about 20-cm. Importantly, the IMF is setup to correct for the Abbe error associated with test article tilting or cupping as a function of temperature.

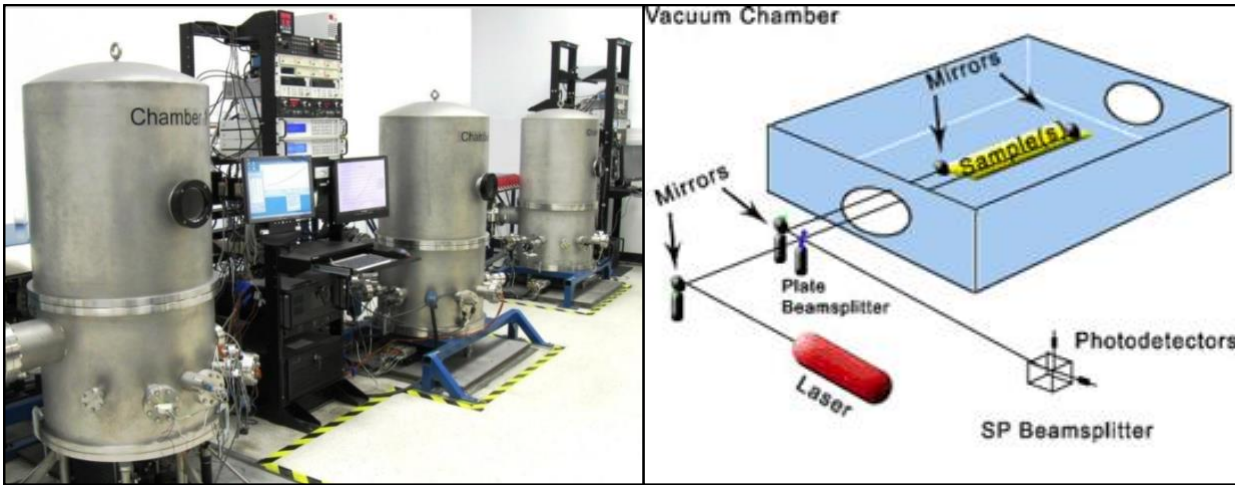

Figure 3-1. Northrup Grumman's Interferometric Metrology Facility, or IMF uses vacuum chambers and differential interferometry, and can test from 20 K to 450 K, depending on the size of the test article, to an accuracy of better than one micron.

3.3 Prototypes & Test Articles

3.3.1 Longeron Assembly

Figure 3-2 details the full scale longeron prototype design that is medium fidelity with all dimension critical features. Longeron assemblies comprise a circular CFRP tube and metallic petal interface fittings. Note that the flight longeron baseline design is a square tube and cross-section geometry remains an open trade study. For this program, a circular cross-section was an important testability consideration, because the IMF is especially sensitive to the tip/tilt that often occurs in non-axisymmetric test articles. The critical dimension is between boreholes of the end-fittings that are used to pin it to the node assemblies on either end. This critical dimension is nominally 98-cm to match the flight design and represents about 75% of the overall 130-cm truss-bay length. Each of 2 longeron prototypes is cut into 3 test articles to fit in the IMF facility as shown in Figure 3-3.

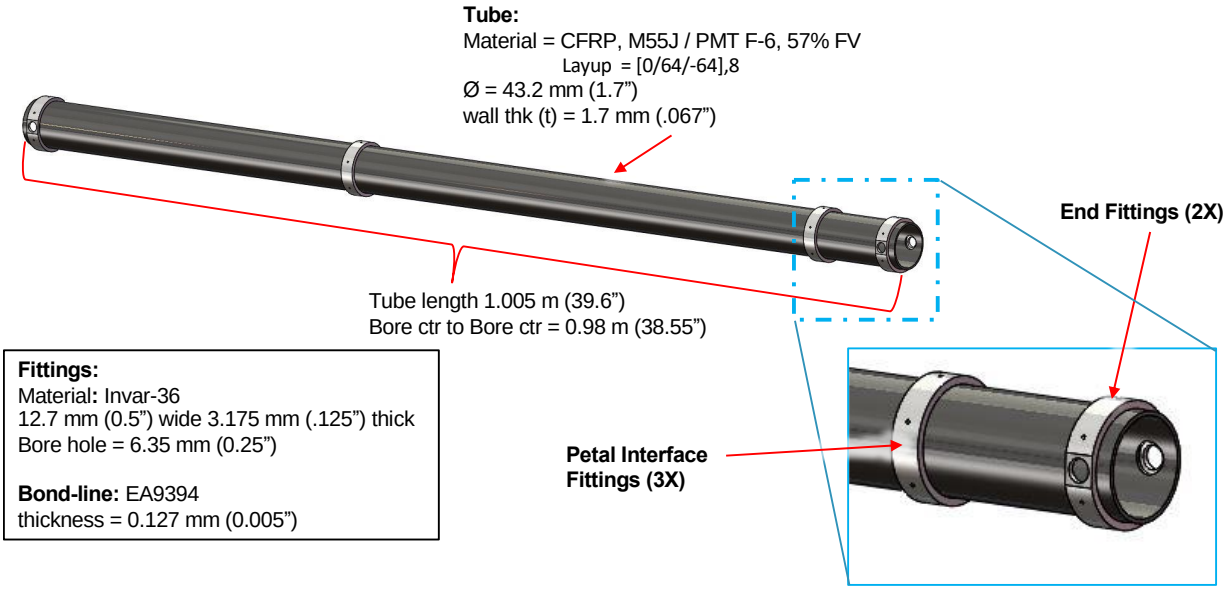

Figure 3-2. Longeron assembly test article final detailed design includes all necessary fittings in the critical dimension load path.

The longeron assembly was manufactured in two stages, the CFRP tube and fittings were manufactured in parallel, and then the fittings were precision injection bonded to the tube. The ply layup orientation and autoclave process that produced the CFRP tube, were the most critical manufacturing steps. The resultant ply-angles and fiber-volumes were precisely measured and used as inputs to the analysis model. Three prototypes were built: SN002 and SN003 were used to satisfy this milestone, and SN001 was utilized exclusively for milestone 7a.

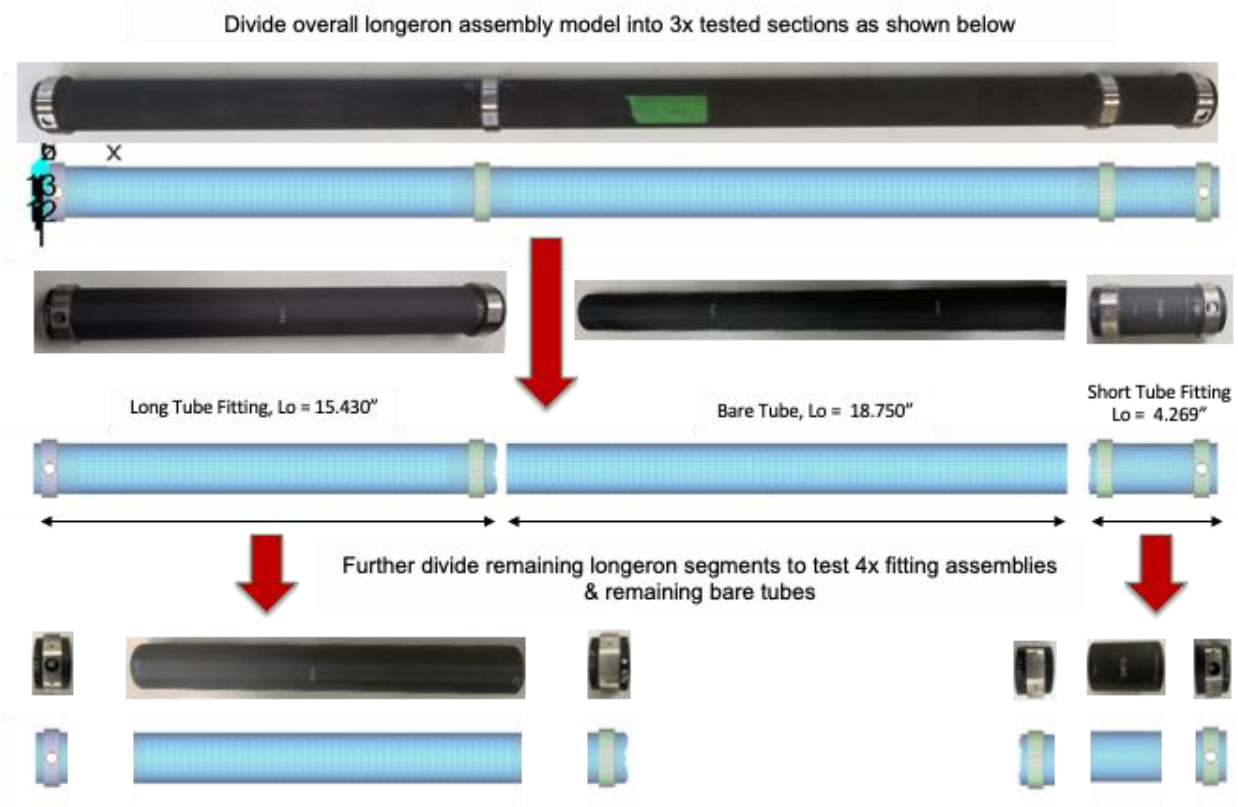

Figure 3-3. Longeron assembly hardware and FEM divided into three test articles to fit in the IMF facility for initial testing, and then further subdivided and measured to understand the individual joint and tube contributions to the assembly for correlation purposes.

3.3.2 Node Assembly

A node assembly spans two truss-bays, and the half-width of the node constitutes its contribution to thermal strain of an individual truss-bay, Figure 2-2. The critical dimension of the half-width of the node assembly is between the bore-hole for the longeron pin, and the node center-line, and is nominally 28-cm. Figure 3-4 displays a full node, and illustrates the manner in which a half-node is separated out to create the prototype, as well as indicating the critical dimension of the wide and narrow side of the node. The narrow side of the node is a simpler, and shorter version of the wide side of the node, and is validated by virtue of the test articles from the wide side. Because of its size, the narrow side has a minor contribution to performance. It should be noted that the node assembly prototype is sized to be compatible with the longeron prototype test article, and both are compatible with the flight requirements.

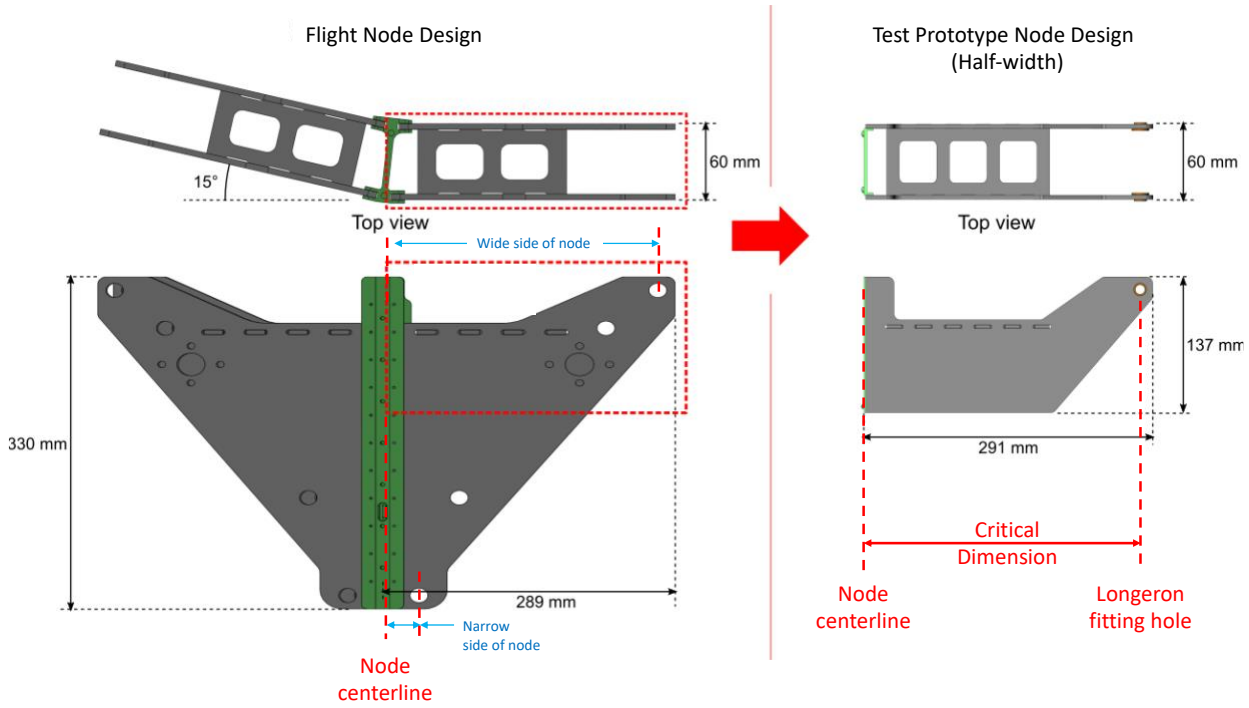

Figure 3-4. Left: flight node assembly baseline design outlining the dimension-critical portion to the truss-bay. Right: Node prototype design, which represents half the overall width of a node-assembly.

Because of asymmetries, neither a full-node or half-node assembly is testable in the IMF, due to the 15° angle between neighboring truss-bays, so for milestone 8a, we test the length-critical joint assemblies that drive the node thermal strain, and that are testable in the IMF. Specifically, we test: 1) the center-brace portion of the node assembly prototype, as cut out of the prototype, and 2) bushing joint assemblies (4x) as bonded into a CFRP layup of node side-plate material, see Figure 3-5 and Figure 3-6. In addition, we test material coupons from the CFRP laminate plate from which the nodes are made.

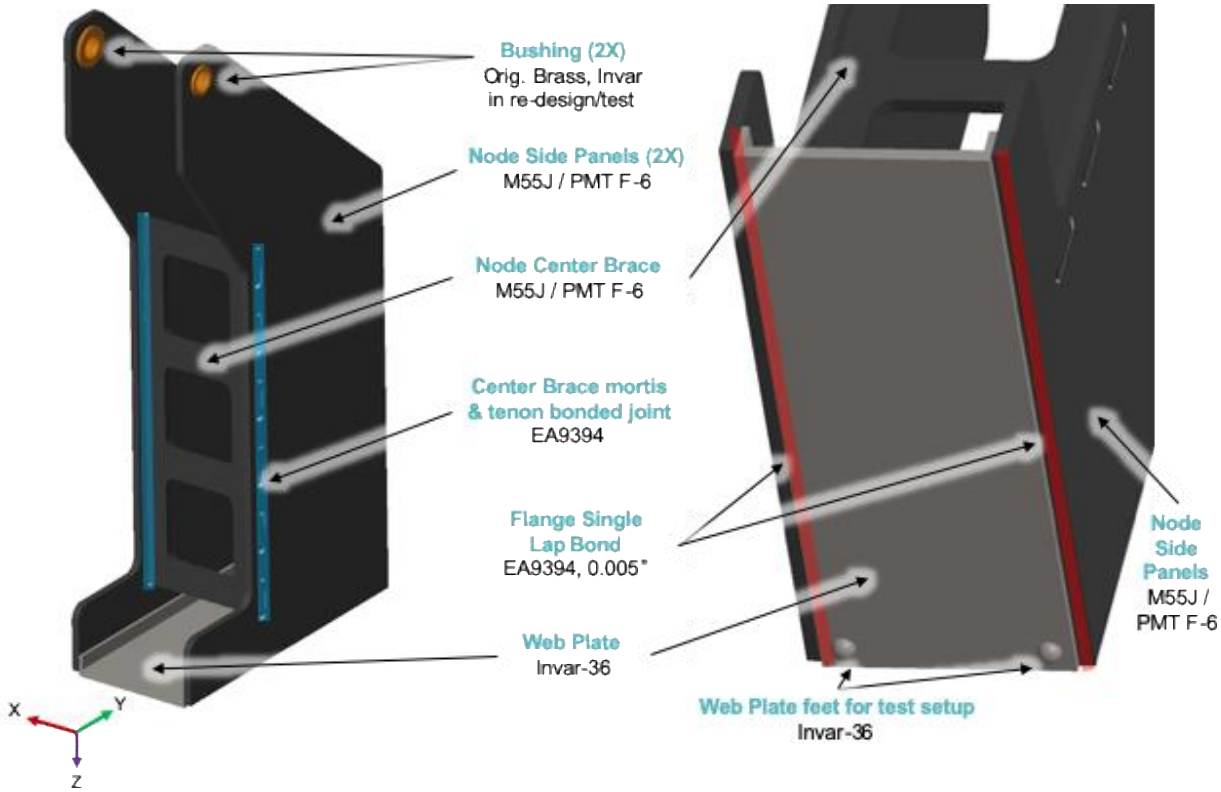

Figure 3-5. Half-width node assembly prototype detailed design includes all necessary fittings and features to represent the critical dimension of the flight design. The center-brace portion of the prototype was cut out for critical dimension testing, and 4x bushing assemblies were manufactured and tested as well.

The node assembly was manufactured in two stages, the CFRP laminate plates and fittings were manufactured in parallel, and then the plates and fittings were precision bonded into an assembly. The ply layup orientation, and autoclave process that produced the CFRP laminate plate were the most critical of the manufacturing steps. The resultant ply-angles and fiber-volumes were precisely measured and used as inputs to the analysis model. Three prototypes were built, one of which was used to satisfy this milestone, the other two were used to satisfy milestone 7a.

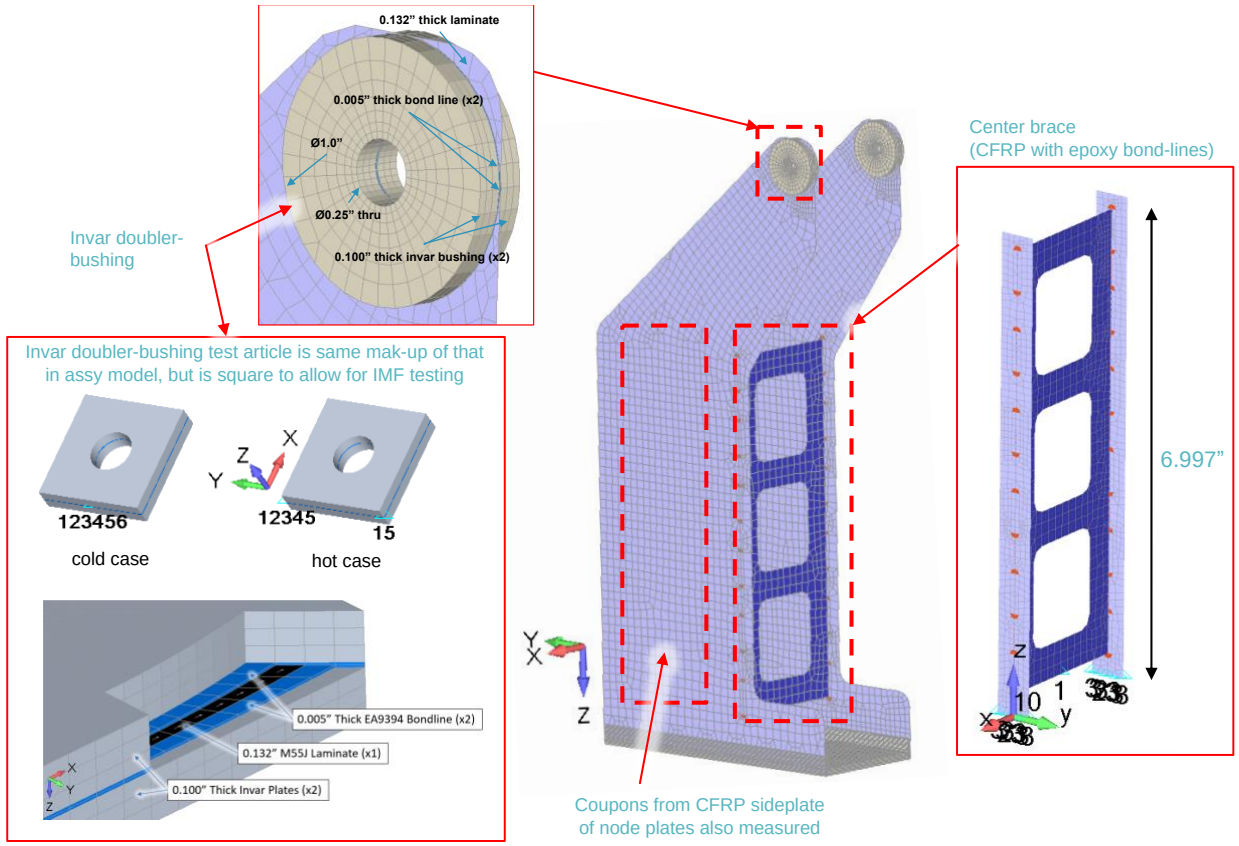

Figure 3-6. Node assembly prototype FEM includes all thermal stability critical features at a high level of fidelity. Also pictured are the breakout joint models of the invar doubler bushing design and center-brace portion of the node assembly, which were used to validate the behavior of the joints assemblies that comprise the overall node assembly thermal strain behavior.

3.4 Test Results Correlation to Prediction

The truss-bay test article results were used as inputs to update the prototype models. The measurement-based thermal strain prediction of the critical dimension is co-plotted with the design curve, and the max expected error bounding curves, Figure 3-7 and Figure 3-8, for the longeron and node, respectively. Note that thermal strain performance is reported in parts per million, the standard unit of measure for thermal strain, and plotted as a function of temperature in °C. Because the longeron represents 75% of the truss-bay, 2 prototypes were tested rather than one, for additional verification. The as-measured length critical dimensions of both longerons are within 1 ppm of their design value, and well within the max expected error across the entire predicted on-orbit observation temperature range of -13 °C and 59 °C, which are also plotted as vertical lines in Figure 3-7.

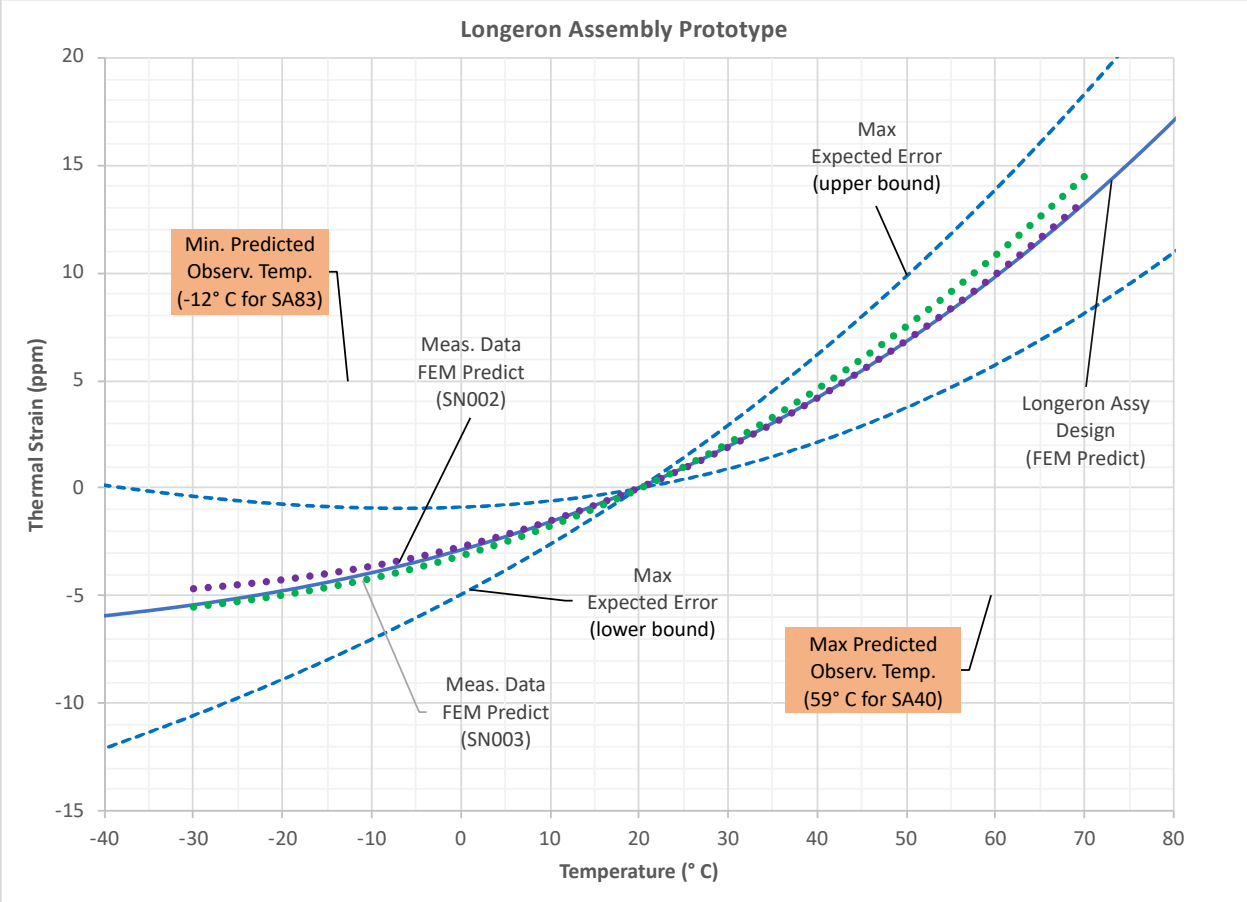

Figure 3-7. Thermal strain vs temperature prediction of the measurement-based FEM of the longeron critical dimension, co-plotted with the design curve, as well the max expected values derived from the error study in section 2.4.

The node assembly analysis model incorporated the results of the joint-level tests. The measurement-based prediction of the critical-dimension thermal strain is plotted in Figure 3-8, and is within the max expected error across the on-orbit observational temperature range. The max error of the measurement-based node model prediction is within 2 ppm of the design for the on-orbit max hot case of 58 °C, and within 1 ppm for max cold case of 9 °C.

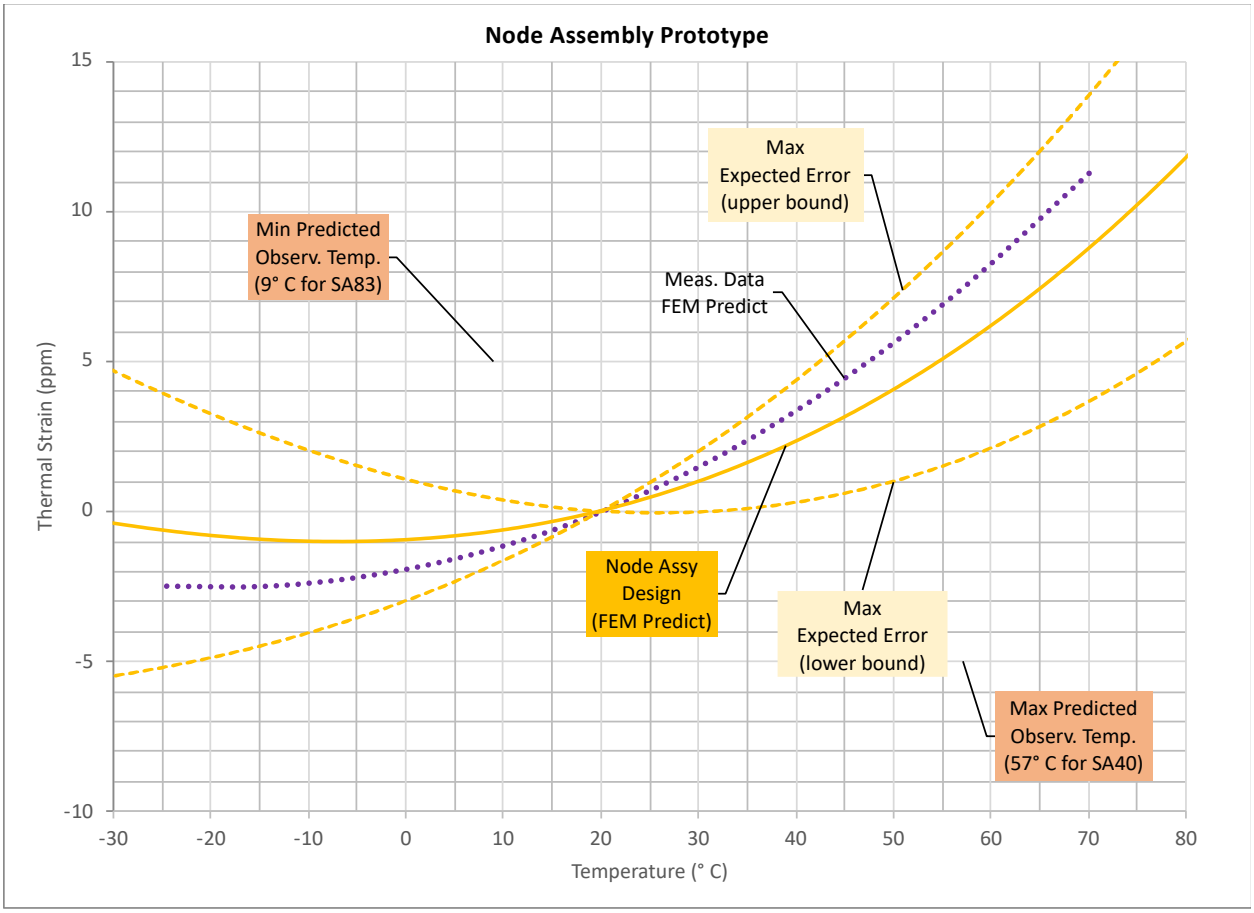

Figure 3-8. Thermal strain vs temperature prediction of the measurement-based FEM of the node assembly critical dimension, co-plotted with the design curve, as well the max expected values derived from the error study in section 2.4.

These results show that with careful design and manufacturing processes, longeron and node assemblies can be manufactured to achieve on-orbit thermal stability performance well within the maximum expected error. Section 5 shows how the longeron and node assembly models use the prototype results as inputs for the flight analysis model to verify on-orbit requirements are met.

4 Flight Design Validated Analysis Model & On-orbit Performance

4.1 Approach

The validated flight analysis model is used to predict disk radius for the thermal environment (sun angle), which is compared to the milestone requirement after adding the max expected error. To that end, the flight analysis model was updated to correlate to the measurement-based prototype predictions, and the corresponding disk radius deformations were computed; both are outlined in this section.

4.2 Analysis Model

A finite element model of the flight Starshade design was built in FEMAP / NX Nastran, Figure 4-1. The key thermal distortion members of the model (petal, truss longerons and truss nodes) used representative element geometry and material properties to match the as-built prototypes, and most importantly, the measured thermal strain as a function of temperature.

Nodal temperatures were mapped for the sun angle cases run on the thermal analysis model, section 2.2. The thermal distortion analysis uses a nonlinear solver that first tensions the spokes to 16 lbf, which puts the truss in compression. The solution then applies the nodal temperatures, and uses the appropriate CTE vs. temperature lookup table to produce the thermal strain, and corresponding thermally induced distortion of the perimeter truss, which is the result we compare to the milestone.

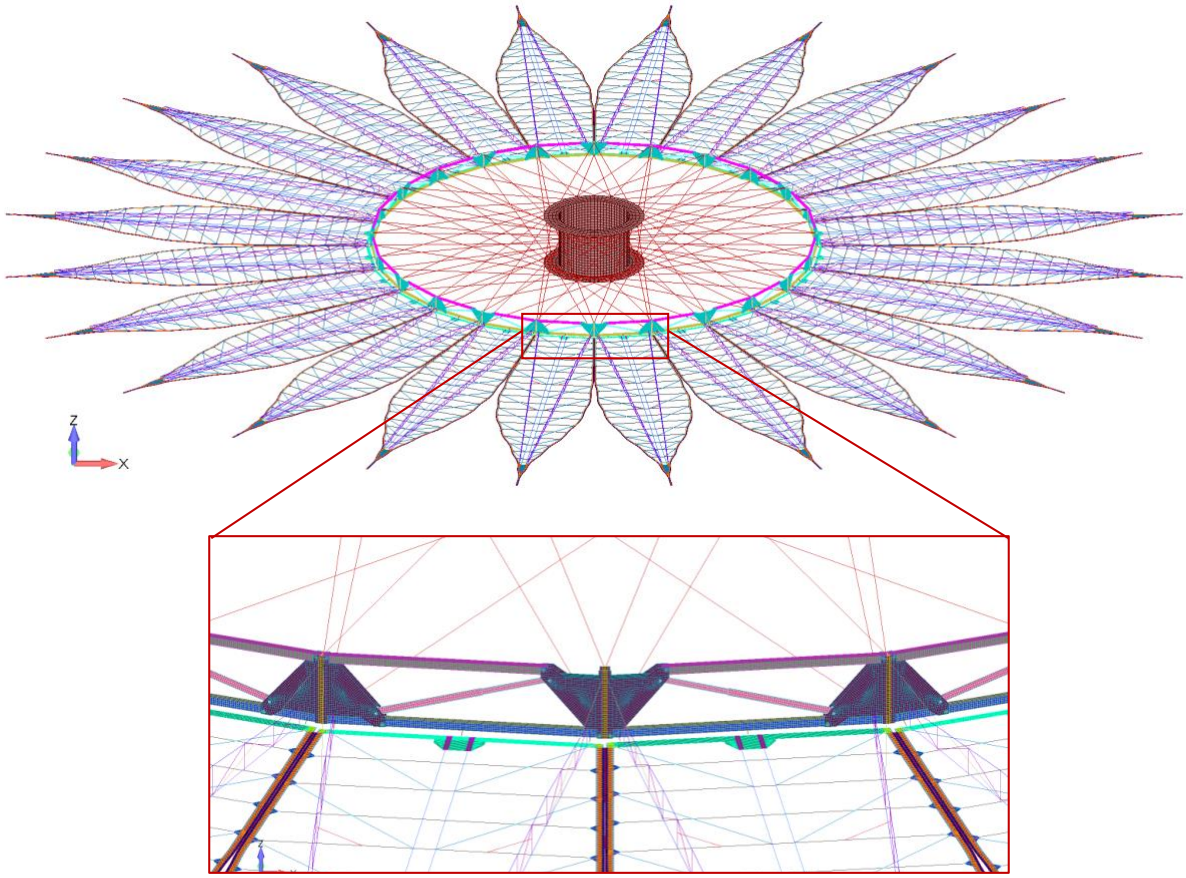

Figure 4-1: Flight design analytical model w/ detail of truss-bay – petal interface

4.2.1 Inner Disk

The IDS structure assembly comprises the hub, spokes, and truss, Figure 2-1. The hub was modeled with laminate elements, and spokes were modeled using beam elements that accurately model their effect on the system, including correlation of the spoke-level load-deflection test results provided by the spoke manufacturer. The truss nodes, longerons, shorterons, and diagonals were modeled using shell elements with 2D orthotropic properties that match component level test values. Each component level material property in the model included CTE as a function of temperature from as-measured component/material level testing performed in this program.

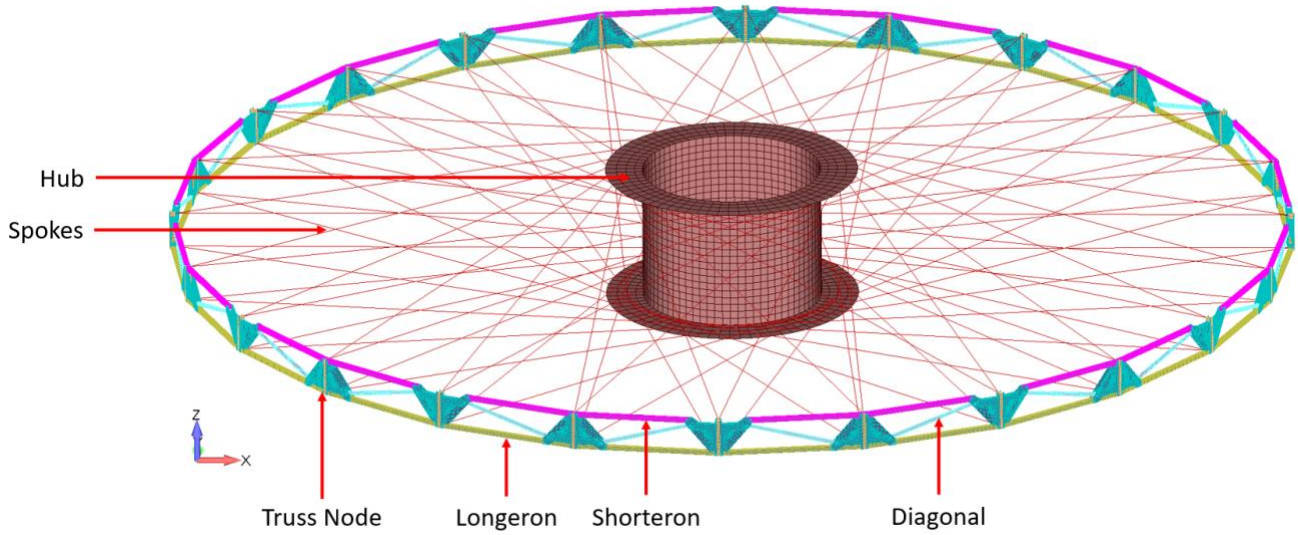

Figure 4-2. Flight inner disk subsystem analytical model

The spokes are connected to the hub and truss nodes with the appropriately released the degrees of freedom that match the flight geometry connection. The longerons, shorterons, and diagonals are connected to the truss node, such that all degrees of freedom are transferred except for rotation about the hinge axis, see Figure 4-3 for component connection locations.

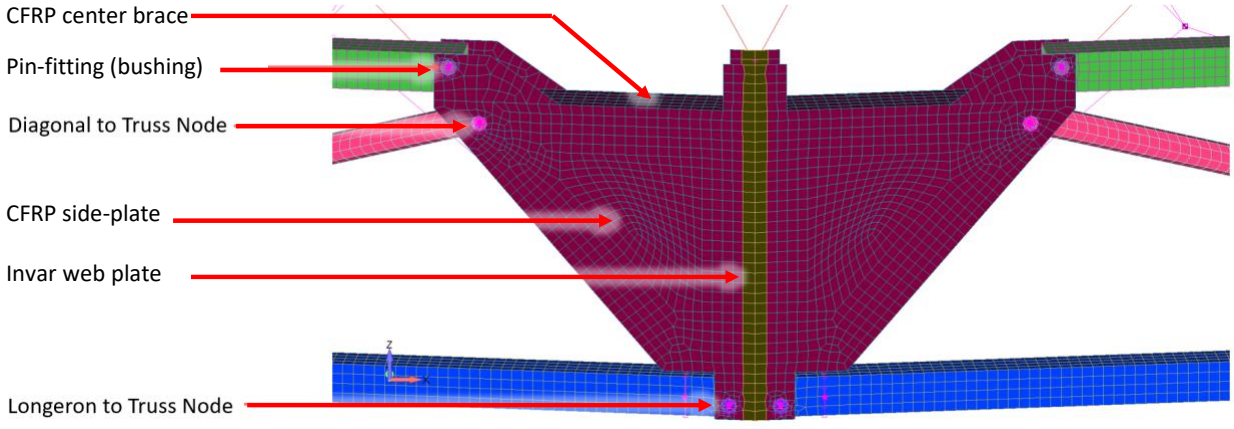

Figure 4-3. Truss-bay FEM component connection details. Shorterons, longerons, and diagonals are free to rotate about their hinge axes.

Figure 4-4 illustrates that each petal is hinged at three locations to the longeron, represented by beam elements, and allows rotation about the base of the petal; the center hinge constrains the petal tangentially. The petal is held in-plane with two struts up to the truss bay. These boundary conditions minimize over-constraining the petal and keep the petal in the starshade plane.

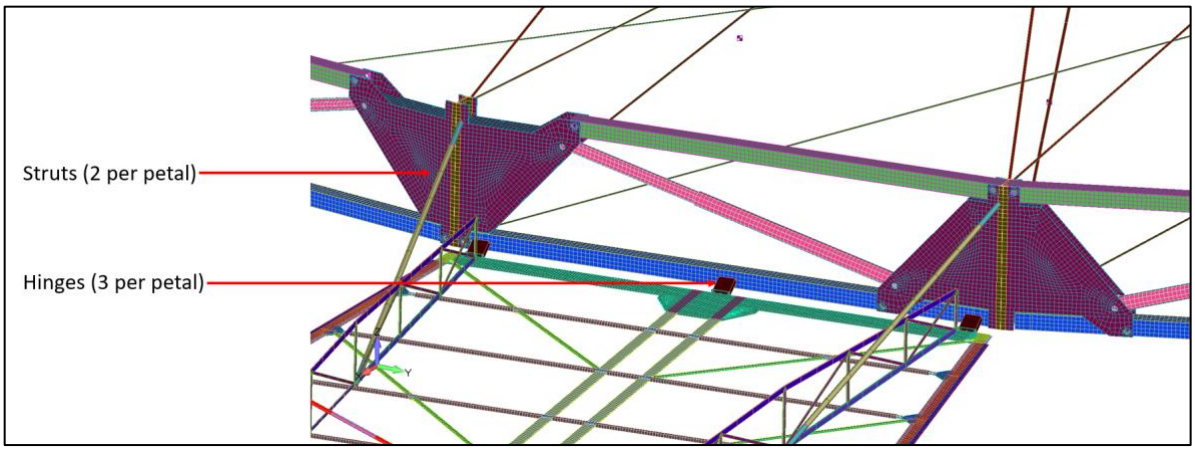

Figure 4-4: Petal connection to perimeter truss

4.2.2 Longeron & Node Assemblies

The longeron is the primary driver of the IDS deflections under thermal load. The longeron prototype test results discussed in section 3.4 were used as an input to this model. The CTE versus temperature of the system level longeron assembly FEM was matched to that of the average of the two as-measured longeron prototypes. Additional verifications against the prototype FEM were performed which found that the overall system level longeron FEM predictions match well with theoretical thermal strain calculations.

The longeron modeled in the flight design system model FEM has a square cross-section, whereas the test hardware used a circular cross-section tube, which was important for test facility considerations, but is not an important consideration for the starshade structural behavior or configuration. The square tubes in the FEM accurately match the behavior of the circular test article, as they match in axial and bending stiffness, and most importantly, the axial thermal strain in the FEM longeron matches the as-tested values.

The truss node also influences IDS thermal deformations, and was modeled to accurately represent the stiffness and thermal strain behavior of the prototype results in section 3.4, but at a lower level of fidelity, to make system model run times reasonable. Included in the model is the Invar web plate, as well as the CFRP plates, and effects of the epoxy bond-lines on the thermal strain performance.

Breakout models of the flight longeron and node assemblies were created to compare to the prototype hardware FEM models to ensure the flight model most accurately reflects the prototype hardware. The comparison showed a small difference, and the flight model was updated to match the prototype hardware stiffness, which had less than a 1% effect on disk radius deformation at temperature.

4.3 On-Orbit Performance Predictions

The validated flight analysis model can now be used to make a measurement-based prediction of the thermal distortion of the actual disk radius design. This is confirmed to fall within the maximum expected error of the actual disk radius design, see Figure 4-5. This is the same

actual disk design curve as that plotted in Figure 2-7, but now with the addition of the maximum expected performance error discussed in section 2.4.

The validated analysis model prediction of actual disk radius falls well within maximum expected error bounds. This was to be expected, given the individual longerons and node validated model prototypes were well within their maximum expected error bounds as well.

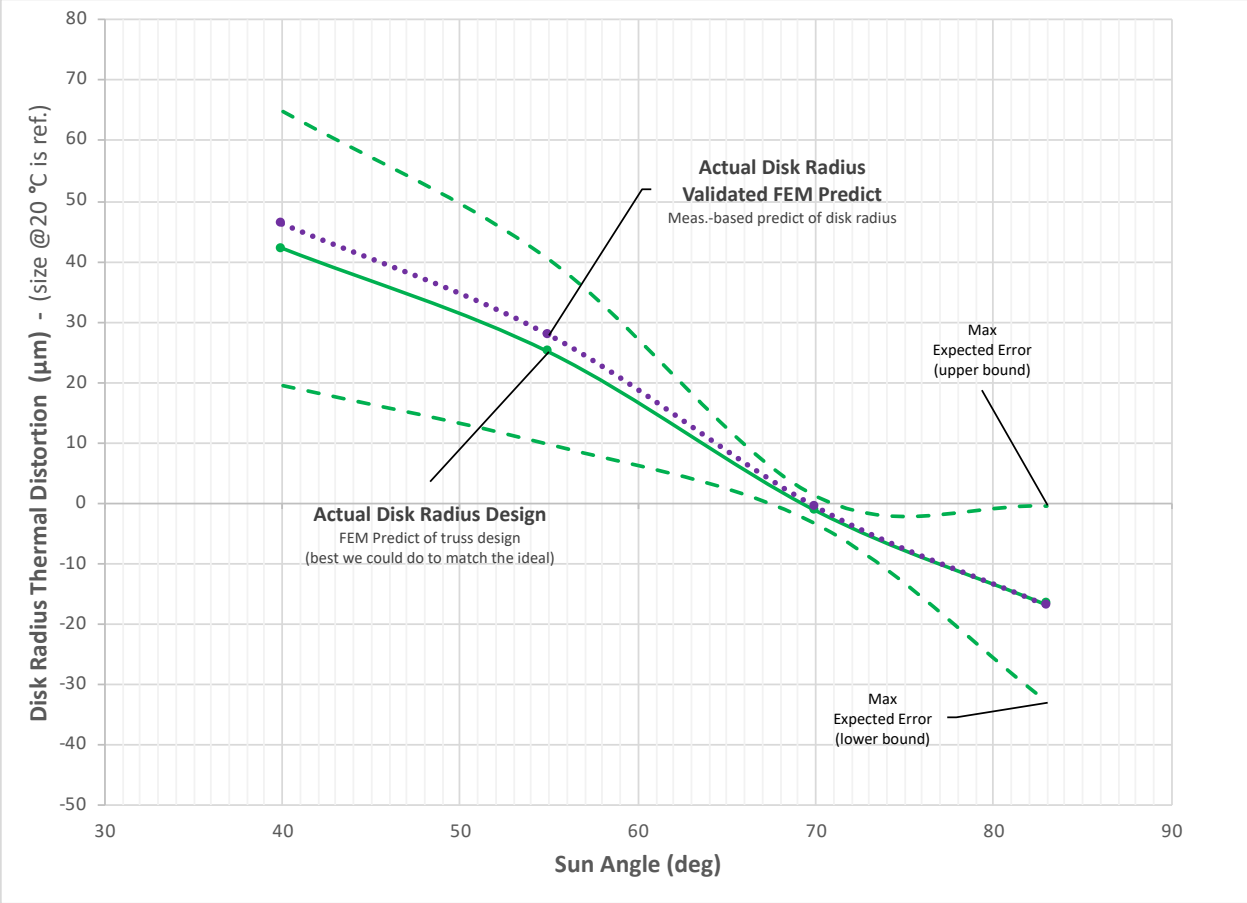

Figure 4-5. Validated flight analysis model prediction of the actual disk radius distortion from nominal, with 20 °C as the reference temperature, for the on-orbit observational sun angle range of 40 to 83 degrees. The max expected performance error bounds are included along with the actual disk radius design.

5 Milestone Analysis & Conclusions

Milestone 8a requires demonstration of on-orbit thermal stability of the petal position radial bias to within ± 50 µm of the ideal disk radius, by analysis, using a validated model of critical dimension vs. temperature. This specification applies as the difference between the actual disk radius and the ideal disk radius, in the thermal environment. In satisfying this requirement, per discussion in section 1, the random radial and tangential requirements are also met.

In order to compare the validated model results to the milestone, the actual disk radius presented in Figure 4-5 must be subtracted from the ideal disk radius of Figure 2-7; this provides the difference in the actual disk radius design from the ideal. The result is plotted in Figure 5-1, with error in actual disk radius from the ideal along the y-axis in micrometers, and the sun angle thermal environment along the x-axis in degrees. The actual disk radius design, the measurement-based FEM prediction of the actual disk radius, and the maximum expected performance error bounds derived in section 2.4, are all plotted after subtracting out the starshade ideal disk radius vs sun angle curve. The resulting residual error can now be directly compared to milestone requirement of ± 50 µm.

We find, as expected, that the maximum error is at the extremal sun angles of 40 and 83 degrees, and the driving case is the SA40 hot-case, where the max expected disk radius error is 26 µm from the ideal disk radius; this results in a margin of 24 µm against the ± 50 µm requirement. The validated model prediction of the actual disk radius design is well centered on the max expected error and the max allowable error. An adjustment in the design would only improve margin by 3 µm, which is less than 10% of the requirement. Interesting to note, the max expected error is always non-zero for our case, and is smallest at SA70. This is because the longeron and node both have a thermal strain reference temperature of 20 °C, which occurs at different sun angles for each of those components.

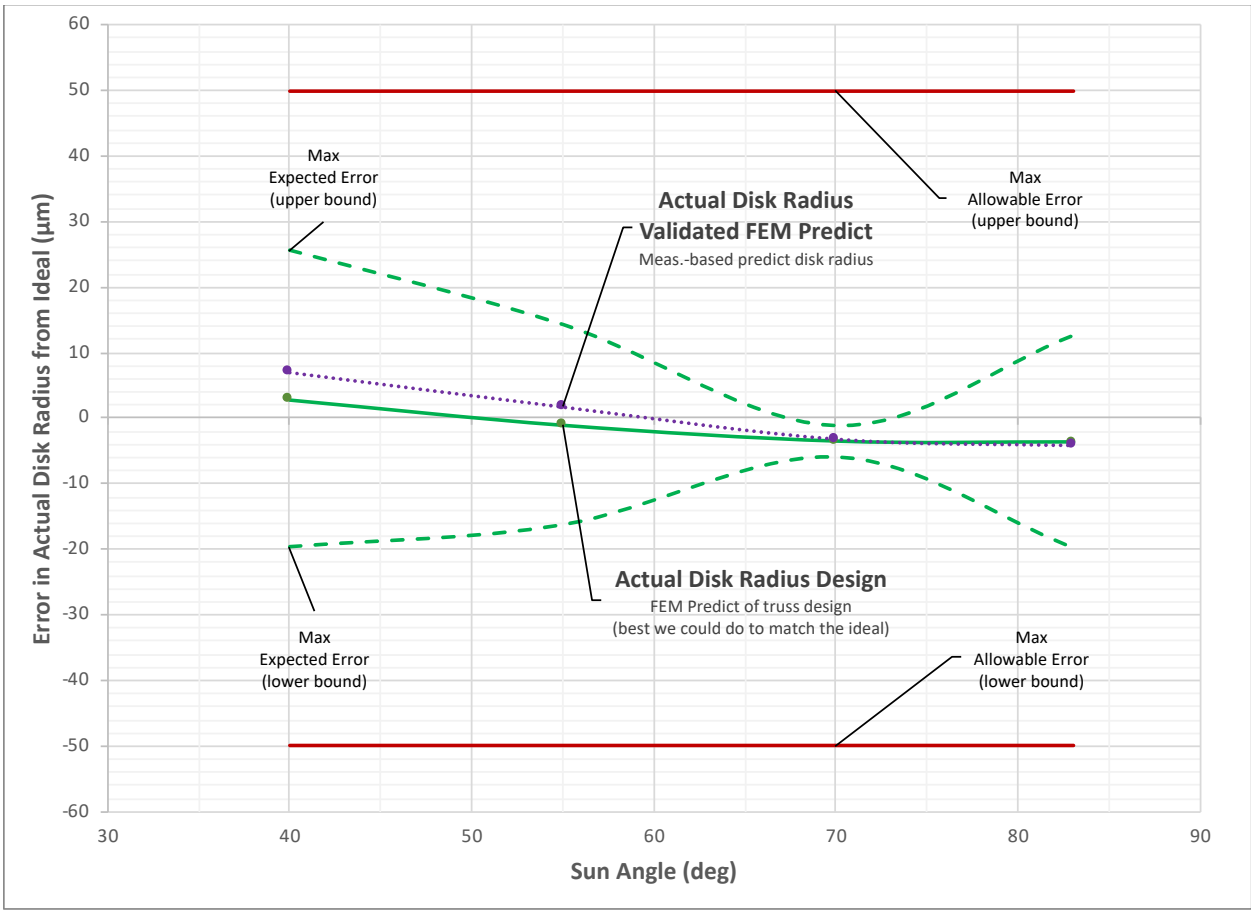

Figure 5-1. The error in actual disk radius design from the ideal is plotted in µm on the y-axis as a function of sun angle in degrees for the on-orbit thermal environment. The ideal disk radius is at y = 0 for all sun angles, which would represent an error of 0 µm from the ideal disk radius. The validated flight design analysis model prediction is co-plotted with the actual disk radius design value and max expected performance error for comparison to the overall requirement of ± 50 µm.

5.1 Future Work

The thermal stability performance result of milestone 8a establishes large margins with respect to the requirement, and puts the program on strong footing going into milestone 8b, which tests an integrated truss-bay that includes all features for thermal stability.

There are three critical aspects of milestone 8b that are not addressed by 8a, and are therefore the focus of near-term future work. These are the detailed understanding and design of 'all features', which by definition, encompass many aspects of the design which have not been fleshed out in doing the initial thermal stability performance design. The second is the metrology system to test an integrated truss-bay assembly. For the limited scope of interim milestone 8a, it was sufficient to design the test articles to match existing facilities. For milestone 8b, a custom metrology setup needs to be designed well before the hardware is in production. Lastly, the program needs to consider the interfaces between the truss and the petal, and how they interact. Modelling will be performed to understand how the interfaces between the petal and truss affect performance, and this will be taken into consideration for the future test campaign.

Acknowledgements

Special thanks to the tremendous efforts of all the engineers, scientists and contributors to the various engineering efforts described in this report, including the teams at JPL, Tendeg, Applied Composites, and Northrup Grumman.

This research was carried out at the Jet Propulsion Laboratory, California Institute of Technology, under a contract with the National Aeronautics and Space Administration.

Acronyms

CFRP	Carbon Fiber Reinforced Polymer
CLT	Classical Laminate Theory
CTE	Coefficient of Thermal Expansion
FEM	Finite Element Model
IMF	Interferometric Measurement Facility
IDS	Inner Disk Subsystem
MUF	Model Uncertainty Factor
PLUS	Petal Launch Restraint and Unfurl Subsystem
PPM	Parts Per Million
RPM	Revolutions per Minute

References

1. Willems, P., “Starshade to TRL5 (S5) Technology Development Plan,” Tech. rep., Jet Propulsion Laboratory, Dec. 2018.
2. Seager, S., Kasdin, N. J., et al., “Starshade Rendezvous Probe Study Report,” Tech. rep., Feb. 2019.
3. Gaudi, S., Seager, S., et al., "HabEx: Habitable Exoplanet Observatory Final Report," Tech. rep., Aug. 2019.
4. Hirsch, B., Webb, D., and Thomson, M., “Starshade Deployable Inner Disk Structure Design and Development,” 3rd AIAA Spacecraft Structures Conference, San Diego, California, USA, Jan. 2016

Appendix A

The starshade must operate in a range of thermal environments, and a small amount of thermal expansion and contraction of the starshade is unavoidable. Given this, the S5 design philosophy is to design the starshade so that the thermal deformations that do occur, have the smallest possible effect on the instrument contrast. A starshade that expands and contracts uniformly over its entire surface would be nearly ideal, and the apodization function is effectively unchanged, except for a shift in the operating wavelengths, that is insignificant for the magnitude of deformation anticipated for this design.

The petal expands differentially between its width and length, so uniform expansion of the starshade is not possible. Our modeling has shown that the instrument contrast degradation is not very sensitive to changes in petal length, and that the contrast change is minimized when the inner disk expands and contracts in the same proportion as the petal width dimension. A 10 ppm expansion of only the inner disk, increases the contrast by 8.5E-13, while a 10 ppm expansion of the petal width alone, degrades the contrast by 9.2E-13. Expanding both the inner disk and petal width simultaneously, degrades the contrast by only 7E-14, a negligibly small amount relative to the overall 1E-10 instrument contrast requirement. Expansion of only the petal length by 10 ppm degrades the contrast by only 1E-14.

Table A-1. Instrument contrast response to perturbations in the starshade

Deformation Term	Delta Strain (ppm)	Delta Instrument Contrast
Disk diameter only (petal position)	10	8.5E-13
Petal width only	10	9.2E-13
Disk diameter & petal width (simultaneously)	10	7E-14
Petal length only	10	1E-14